The signaling lipid sphingosine 1-phosphate regulates mechanical pain

Authors and Affiliations: Rose Z. Hill[1], Benjamin Hoffman[2,3], Takeshi Morita[1#], Stephanie M. Campos[4‡], Ellen A. Lumpkin[2, 4], Rachel B. Brem[5, 6], Diana M. Bautista[1, 4, 7, 8*]

1. Department of Molecular and Cell Biology, University of California, Berkeley, CA 94720, USA.
2. Department of Physiology & Cellular Biophysics, Columbia University College of Physicians & Surgeons, New York, NY 10032
3. Medical Scientist Training Program, Columbia University, New York, NY 10032
4. Neurobiology Course, Marine Biological Laboratory, Woods Hole, MA
5. Department of Plant and Microbial Biology, University of California, Berkeley, CA 94720, USA.
6. Buck Institute for Research on Aging, Novato, CA 94945, USA.
7. Helen Wills Neuroscience Institute, University of California, Berkeley, CA 94720, USA.
8. Lead Contact

[#] Current Address: Rockefeller University, New York, NY 10065, USA.

[‡] Current Address: Indiana University, Bloomington, IN 47405, USA.

[*] Correspondence: dbautista@berkeley.edu

Abstract

Somatosensory neurons mediate responses to diverse mechanical stimuli, from innocuous touch to noxious pain. While recent studies have identified distinct populations of A mechanonociceptors (AMs) that are required for mechanical pain, the molecular underpinnings of mechanonociception remain unknown. Here, we show that the bioactive lipid sphingosine 1-phosphate (S1P) and S1P Receptor 3 (S1PR3) are critical regulators of acute mechanonociception. Genetic or pharmacological ablation of S1PR3, or blockade of S1P production, significantly impaired the behavioral response to noxious mechanical stimuli, with no effect on responses to innocuous touch or thermal stimuli. These effects are mediated by fast-conducting Aδ mechanonociceptors, which displayed a significant decrease in mechanosensitivity in S1PR3 mutant mice. We show that S1PR3 signaling tunes mechanonociceptor excitability via modulation of KCNQ2/3 channels. Our findings define a new role for S1PR3 in regulating neuronal excitability and establish the importance of S1P/S1PR3 signaling in the setting of mechanical pain thresholds.

Introduction

Pain is a complex sensation. It serves to protect organisms from harmful stimuli, but can also become chronic and debilitating following tissue injury and disease. Distinct cells and molecules detect noxious thermal and mechanical stimuli. Thermal pain is detected by thermosensitive TRP channels in subsets of nociceptors[1–4], and gentle touch is detected by Piezo2 channels in low-threshold mechanoreceptors (LTMRs)[5–7]. Aδ high-threshold mechanoreceptors (HTMRs) have been shown to play a key role in responses to painful mechanical stimuli[8–10].

Recent studies have shown that there are at least two populations of HTMRs that mediate responses to noxious mechanical stimuli. The *Npy2r*+ subpopulation of HTMRs mediates fast

65 paw withdrawal responses to pinprick stimulation and terminate as free nerve endings in the
66 epidermis[11]. The *Calca+* subpopulation of circumferential-HTMRs respond to noxious force and
67 hair pulling, and terminate as circumferential endings wrapped around guard hair follicles[12].
68 Additionally, somatostatin-expressing interneurons of laminae I-III in the dorsal horn of the
69 spinal cord receive input from nociceptors and are required for behavioral responses to painful
70 mechanical stimuli[13]. Despite these advances in defining the cells and circuits of mechanical
71 pain, little is known about the molecular signaling pathways in mechanonociceptors.
72
73 Here, we show that the bioactive signaling lipid sphingosine 1-phosphate (S1P) is required for
74 mechanical pain. Mice lacking the S1P receptor S1PR3 display striking and selective deficits in
75 behavioral responses to noxious mechanical stimuli. Likewise, peripheral blockade of S1PR3
76 signaling or S1P production impairs mechanical sensitivity. We found that S1P constitutively
77 enhances the excitability of A mechanonociceptors (AMs) via closure of KCNQ potassium
78 channels to tune mechanical pain sensitivity. The effects of S1P are completely dependent on
79 S1PR3. Our findings uncover an essential role for S1P signaling in noxious mechanosensation.
80

81 Results

82 To identify candidate genes underlying mechanosensation, we previously performed
83 transcriptome analysis of the sensory ganglia innervating the ultra-sensitive tactile organ (the
84 star) of the star-nosed mole[14]. Immunostaining revealed the tactile organ is preferentially
85 innervated by myelinated Aδ fibers[14]. While our original analysis focused on ion channels
86 enriched in the neurons of the star organ, our dataset also revealed enrichment of several
87 components of the S1P pathway, including S1PR3. Likewise, single-cell RNA seq of mouse
88 DRG neurons revealed expression of *S1pr3* in neurofilament H-expressing myelinated

89 mechanoreceptors[15], which includes Aβ as well as the Aδ neuronal populations. Thus, we set
90 out to define the role of S1P signaling and S1PR3 in somatosensory mechanoreceptors.
91
92 **S1PR3 mediates acute mechanical pain**
93 We first examined a variety of somatosensory behaviors in mice lacking S1PR3[16]
94 (*S1pr3*$^{tm1Rlp/Mmnc}$; referred to herein as *S1pr3*$^{-/-}$). We initially investigated baseline responses to
95 mechanical stimuli. *S1pr3*$^{-/-}$ mice displayed a dramatic loss of mechanical sensitivity (Fig. 1A),
96 as von Frey paw withdrawal thresholds were significantly elevated in *S1pr3*$^{-/-}$ mice relative to
97 *S1pr3*$^{+/+}$ and *S1pr3*$^{+/-}$ littermates (mean thresholds: 1.737 g vs. 0.736 and 0.610 g, respectively).
98 Moreover, *S1pr3*$^{-/-}$ mice demonstrated decreased responses to a range of noxious tactile stimuli
99 (2-6 g; Fig. 1B) and to noxious pinprick stimulation (Fig. 1C), but normal responsiveness to
100 innocuous tactile stimuli (0.6-1.4g; Fig. 1B). *S1pr3*$^{-/-}$ mice exhibited normal tape removal
101 attempts[6] (Fig. 1D), righting reflexes (Fig. S1A), radiant heat withdrawal latencies (Fig. S1B),
102 and itch-evoked scratching[17] (Fig. S1C). These results demonstrate a selective role for S1PR3
103 in acute mechanical pain.
104
105 As a complement to our analysis of somatosensation in *S1pr3*$^{-/-}$ animals, we employed a
106 pharmacological approach, using the S1PR3-selective antagonist TY 52156 (TY). Similar to the
107 phenotype of knockout animals, intradermal injection of 500 μM TY into the mouse hindpaw (the
108 site of testing) triggered a rapid and significant elevation in von Frey paw withdrawal thresholds
109 (Fig. 1E) and decreased responsiveness to noxious (2-6 g), but not innocuous (0.6-1.4g), tactile
110 stimuli (Fig. 1F). In contrast, blockade of S1PR1 with the selective antagonist W146 had no
111 effect on mechanical thresholds (Fig. 1E). Overall, these data show that S1PR3 signaling sets
112 mechanical pain sensitivity.
113
114

115 **Endogenous S1P mediates acute mechanical pain**

116 We next asked whether peripheral S1P was required for the S1PR3-dependent effects on
117 mechanosensation. We decreased S1P levels via injection of the sphingosine kinase inhibitor
118 SKI II to block local production of S1P[18] or elevated S1P levels via intradermal injection of S1P
119 and measured behaviors 30 minutes after injection. Decreasing local S1P levels significantly
120 reduced mechanical sensitivity (Fig. 2A), comparable to the hyposensitivity phenotype observed
121 in *S1pr3*$^{-/-}$ mice (Fig. 1A). Again, similar to what was observed in *S1pr3*$^{-/-}$ animals (Fig. S1B),
122 peripheral blockade of S1PR3 or S1P production had no effect on thermal sensitivity (Fig. S1D).
123 Surprisingly, injecting exogenous S1P (10 μM; maximum solubility in saline vehicle) had no
124 effect on mechanical sensitivity (Fig. 2A-B). However, as previously reported[19], S1P injection
125 triggered thermal hypersensitivity (data not shown) demonstrating that the lack of effect on
126 mechanical hypersensitivity is not due to problems with S1P delivery or degradation. Although
127 quantification of native S1P levels in skin is inaccurate owing to avid lyase activity[20], our data
128 establish that baseline S1P levels are sufficient to maximally exert their effect on S1PR3-
129 dependent mechanical pain, such that increased levels of S1P do not evoke mechanical
130 hypersensitivity, but diminished S1P leads to mechanical hyposensitivity. These data show that
131 constitutive S1PR3 signaling is required for normal mechanosensitivity.

132

133 **S1PR3 is expressed in A mechanonociceptors**

134 We next aimed to characterize the somatosensory neuron subtypes expressing *S1pr3* as a
135 window onto the role of S1PR3 in acute mechanical pain. We used *in situ* hybridization (ISH)
136 with a specific *S1pr3* probe to examine expression patterns of *S1pr3*. In our experiments, 43%
137 of cells from wild-type dorsal root ganglia (DRG) expressed *S1pr3* (Fig. 3A; top, Fig. 3E). We
138 observed no reactivity in DRG isolated from *S1pr3*$^{-/-}$ mice (Fig. 3A; bottom), and no significant
139 differences in the distribution of cell sizes between *S1pr3*$^{-/-}$ and *S1pr3*$^{+/+}$ ganglia (p = 0.18;
140 Kolmogorov-Smirnov type II test), suggesting no loss of major neuronal subtypes. While a

141 previous study using antibody staining concluded that S1PR3 protein was expressed by all DRG
142 neurons[21], we found that anti-S1PR3 antibodies showed broad immunoreactivity in DRG from
143 mice lacking S1PR3 (data not shown).
144
145 Co-ISH revealed that a population of *S1pr3*+ neurons represents Aδ mechanonociceptors
146 (AMs). These cells were medium-diameter (25.9 ± 4.5 μm) and expressed *Scn1a* (39.9% of all
147 *S1pr3*+; Fig. 3B-C), a gene that encodes the Nav1.1 sodium channel which mediates
148 mechanical pain in Aδ fibers[10], as well as *Npy2r* (20.4% of all *S1pr3*+; Fig. 3B-C), a marker of a
149 specialized subset of mechanonociceptive A fibers[7]. *S1pr3* was expressed in 70.6% of *Scn1a*+
150 cells and 72% of *Npy2r*+ cells, comprising a majority of both these populations. Interestingly, a
151 substantial subset of cells co-expressed *S1pr3* and the mechanically sensitive channel *Piezo2*
152 (Fig. 3C), which is expressed in Aβ, Aδ, and C fibers[6]. The remaining *S1pr3*+ cells were small
153 diameter (23.4 ± 8.2 μm), *Trpv1*+ C nociceptors (27.3% of total cells). To elucidate the role of
154 S1PR3 in mechanical pain, we focused our analysis on Aδ mechanonociceptors, as C-fibers do
155 not contribute to baseline mechanical thresholds[22].
156
157 We also used an *S1pr3*$^{mCherry/+}$ reporter mouse[23] as an independent strategy to explore *S1pr3*
158 expression and localization. Analysis of this line detected expression of S1PR3-mCherry fusion
159 protein in 48.3% of cultured DRG neurons (Fig. 3E), mirroring the results from ISH. Additionally,
160 we observed S1PR3 expression in nerve fibers that innervate the skin using antibodies against
161 mCherry in whole-mount immunohistochemistry (Fig. 3D). We observed overlap of S1PR3-
162 expressing free nerve endings with NefH+ myelinated A fibers, but did not observe expression
163 of S1PR3 in circumferential hair follicle receptors (Fig. 3D). These results suggest that S1PR3 is
164 not expressed in the circ-HTMR subpopulation of mechanonociceptors identified by Ghitani *et*
165 *al.* In addition to our mRNA and protein localization experiments, calcium imaging revealed that

166 a subset of S1PR3+ neurons were activated by the Nav1.1-selective toxin Hm1a[10] (Fig. 3E). We
167 conclude that a subset of *S1pr3*+ neurons represents AMs that terminate as free nerve endings.
168

169 **S1PR3 is required for nociceptive responses of high-threshold AM nociceptors**

170 Given that the behavioral deficit of *S1pr3*$^{-/-}$ animals was restricted to noxious mechanosensation,
171 we utilized *ex vivo* skin-nerve recordings to analyze the effects of genetic ablation of S1PR3 on
172 AM afferents, which mediate fast mechanical pain sensation (Fig. 4A). We hypothesized that
173 S1PR3 may play a role in AM afferent function. Strikingly, the median von Frey threshold to
174 elicit firing in AM nociceptors was significantly higher in *S1pr3*$^{-/-}$ animals (3.92 mN) compared to
175 littermate controls (1.56 mN; Fig. 4C). Additionally, *S1pr3*$^{-/-}$ AM nociceptors displayed reduced
176 sensitivity in their force-response relation (slope for $^{+/-}$ versus $^{-/-}$: 50 Hz/N versus 35 Hz/N), as
177 well as attenuated firing over the noxious, but not innocuous, range of mechanical stimulation
178 (Fig. 4D). Furthermore, *S1pr3*$^{-/-}$ AM nociceptors displayed a right-shifted cumulative response
179 curve (50% effective force for $^{+/-}$ versus $^{-/-}$: 33.7 versus 60.0 mN; Fig. 4E), consistent with the
180 mechanonociceptive hyposensitivity observed *in vivo*. A recent report suggested that A-
181 nociceptors are composed of two distinct neuronal populations that differ genetically, in
182 mechanically evoked response patterns, and in conduction velocity[11]. Accordingly, we found
183 that a proportion of AM nociceptors, characterized by adapting responses to static mechanical
184 stimuli (Adapting AM), were selectively lost in *S1pr3*$^{-/-}$ animals (Fig. 4F-G). However, we found
185 no differences in conduction velocity between genotypes (Fig. 4B). We conclude that S1PR3 is
186 an essential regulator of both mechanical threshold and sensitivity in a distinct population of AM
187 nociceptors.
188

189 **S1PR3 modulates KCNQ2/3 channels to regulate AM excitability**

190 To define the molecular pathway(s) by which S1PR3 modulates mechanonociceptor function,
191 we next examined S1P signaling in cultured DRG neurons. Unlike the environment of sensory

192 neurons in intact skin, the physiological Ringer's solutions used *in vitro* lack S1P. Thus for our *in*
193 *vitro* experiments we tested the effects of exogenous S1P on neuronal excitability. We
194 interrogated the molecular mechanism by which S1P signaling regulates mechanical pain using
195 current-clamp recording of medium-diameter *S1pr3*$^{mCherry/+}$ dissociated DRG neurons
196 (membrane capacitance = 61.05 ± 1.92 pF), which ISH identified as putative
197 mechanonociceptors (Fig. 3B-C). In these cells, 1 μM S1P application did not elicit firing in the
198 absence of current injection (Fig. 5A, Fig. S2A). However, S1P dramatically lowered the
199 threshold to fire action potentials (rheobase) in an S1PR3-dependent manner (Fig. 5A, Fig.
200 S2B).
201
202 We then set out to determine how S1PR3 activity increases neuronal excitability using whole-
203 cell voltage clamp recording. While we found that S1P application had no effect on
204 instantaneous sodium currents or steady state potassium currents (Fig. S2C-D), S1P
205 significantly reduced slow, voltage-dependent tail current amplitudes (Fig. 5B; Fig. 5D (top)) in
206 an S1PR3-dependent manner (Fig. 5B, center).
207
208 As tail currents in Aδ neurons are primarily mediated by KCNQ2/3 potassium channels[24], we
209 postulated that S1P might alter tail currents through modulation of these channels. To address
210 whether KCNQ2/3 channels mediated S1P-dependent neuronal excitability, we examined
211 several other aspects of the S1P-sensitive current. S1P triggered a robust increase in input
212 resistance (Fig. 5E), consistent with the closure of potassium channels. Likewise, I-V analysis
213 revealed that the current inhibited by S1P application was carried by potassium (Fig. 5F).
214 Additionally, the lack of an effect of S1P on resting membrane potential (Fig. S2E) and steady
215 state potassium current (Fig. S2D) were consistent with the electrophysiological properties of
216 KCNQ2/3 channels in DRG neurons[24–27]. Finally, application of the KCNQ2/3-selective inhibitor
217 linopirdine completely occluded the effects of S1P on tail current (Fig. 5C, Fig. 5d (bottom)).

218 These findings are consistent with S1P/S1PR3-dependent inhibition of KCNQ2/3 in
219 somatosensory neurons.
220
221 We also found that the effect of S1P on KCNQ2/3 currents was mediated by low levels of S1P,
222 exhibiting an IC_{50} of 48 nM with saturation at 100 nM (Fig. S2F). While S1P cannot be
223 accurately measured in non-plasma tissues, this is similar to estimated levels of S1P in
224 peripheral tissues[28,29]. Thus, our *in vitro* IC_{50} supports our behavioral observations that baseline
225 S1P levels are sufficient to maximally exert their effect on mechanical pain. In summary, our
226 electrophysiological and behavioral observations support a model in which baseline S1P/S1PR3
227 signaling governs mechanical pain thresholds through modulation of KCNQ2/3 channel activity
228 in AM neurons (Fig. 6).
229

230 Discussion

231 This study identifies S1P/S1PR3 as a key pathway that tunes mechanical pain sensitivity.
232 Recent studies have identified distinct populations of AM nociceptors that are required for
233 mechanical pain[11,12]. Likewise, it was discovered that a subset of somatostatin-expressing
234 spinal interneurons are required for mechanical pain transduction[13]. While these papers
235 delineate the cells and circuitry of mechanical pain, the molecular underpinnings of
236 mechanonociception in these neurons were unknown. We now demonstrate that S1PR3 is
237 required for normal mechanosensitivity in a majority of mechanonociceptors, including the
238 *Npy2r*+ population, recently identified by Arcourt *et al.,* that innervates the epidermis and
239 encodes noxious touch[11].
240
241 While the transduction channels that detect noxious force remain enigmatic, we show that
242 S1PR3 signaling modulates KCNQ2/3 channels to regulate excitability of mechanonociceptors

243 (Fig. 6). GPCR-mediated inhibition of KCNQ2/3 potassium channels is a well-known mechanism
244 by which neuronal excitability is regulated[30]. Other studies have shown that KCNQ channels
245 mediate excitability of Aδ fibers[24] and that opening KCNQ2/3 channels directly with retigabine
246 alleviates pain *in vivo*[25,31,32]. Our results not only complement previous work implicating
247 KCNQ2/3 channels in pain, but also define the upstream mechanisms that promote the
248 regulation of KCNQ2/3 channels to tune mechanical pain thresholds. Our data thus highlight
249 S1PR3 as a novel and attractive target for the treatment of mechanical pain and describe a new
250 signaling pathway by which S1P regulates AM nociceptor excitability.
251
252 Interestingly, the neurons that innervate the ultra-sensitive tactile organ of the star-nosed mole
253 are highly enriched in transcripts for S1PR3 and KCNQ channels, as well as for a variety of
254 other potassium channels[14]. While it is difficult to directly examine the physiological basis for
255 heightened mechanosensitivity in the star-nosed mole, S1PR3-dependent modulation of KCNQ
256 may represent an important mechanism underlying the high tactile sensitivity of the star organ.
257
258 Outside of the nervous system, S1P signaling via S1PR1 allows for the continuous circulation of
259 lymphocytes between blood, lymph, and peripheral tissues[33]. Our findings that S1P plays a key
260 role in somatosensation is in line with recent studies showing that sensory neurons co-opt
261 classical immune pathways to drive chronic itch or pain[34,35]. What distinguishes this study from
262 the others is that S1P signaling is critical for acute mechanical pain, even in the absence of
263 inflammation. In the immune system, disruptions in S1P levels or S1PR1 signaling results in
264 significant immune dysfunction and disease[36–38]. Paralleling the role of S1PR1 in the immune
265 system, we propose that S1PR3 might constitutively regulate the excitability of a variety of
266 neurons and that aberrant S1P signaling may trigger nervous system dysfunction and disease.
267 For example, S1P has been proposed to constitutively modulate synaptic transmission and
268 excitability of hippocampal neurons in slice recordings via S1PR3[39–42], and S1PR3-deficient

269 animals display learning and memory deficits[39]. However, these previous studies, unlike ours,
270 did not identify a molecular mechanism by which S1P signaling alters neuronal activity.
271 Abnormal S1P signaling is also linked to a host of neurological disorders, including thermal
272 hypersensitivity[19], multiple sclerosis[43], Huntington[44], Parkinson's[45], and Alzheimer's disease[46].
273 In addition to expression in the somatosensory system, S1PR3 is expressed in brain regions
274 relevant to these disorders (Allen Brain Atlas) and may thus represent an important mechanism
275 by which S1P signaling regulates excitability.
276
277 The relationship between lipids and ion channel activity in the context of mechanotransduction
278 is well-established and thought to occur through direct channel-lipid interactions[47,48]. Here, we
279 highlight the importance an indirect pathway in which a lipid activates a GPCR to modulate
280 mechanoreceptor activity. Our findings complement very recent work demonstrating the diverse
281 and complex roles that GPCRs play in somatosensory signaling[49]. Our study demonstrates a
282 crucial role for S1P signaling in the peripheral nervous system and highlights the potential of
283 S1PR3 as a target for new therapies for mechanical pain.
284

285 Materials and Methods

286 *Behavioral studies & mice*

287 *S1pr3*$^{mcherry/+}$ and *S1pr3*$^{-/-}$ mice were obtained from Jackson Laboratory and backcrossed to
288 C57bl6/J. Wherever possible, wild-type/heterozygous (*S1pr3)* littermate controls were used in
289 behavioral experiments. Mice (20–25 g) were housed in 12 h light-dark cycle at 21°C. Mice were
290 singly housed one week prior to all behavioral experiments and were between 8-10 weeks at
291 the time of the experiment. All mice were acclimated in behavioral chambers on 2 subsequent
292 days for 1 hour prior to recording for itch behavior, von Frey, and radiant heat.
293

294 Itch and acute pain behavioral measurements were performed as previously described[50,51]. Mice
295 were shaved one week prior to itch behavior. Compounds injected: 500 μM TY 52156 (Tocris),
296 50 μM SKI II (Tocris), 10 μM S1P (Tocris, Avanti Polar Lipids), 50 mM chloroquine (Sigma), and
297 27 mM histamine (Tocris) in PBS with either DMSO- or Methanol-PBS vehicle controls.
298 Pruritogens were injected using the cheek model (20 μL) of itch, as previously described[52].
299 Behavioral scoring was performed while blind to experimental condition and mouse genotype.
300 All scratching behavior videos were recorded for 1 hour and scored for the first 30 minutes. Bout
301 number and length were recorded.
302
303 For radiant heat and von Frey hypersensitivity behavior, drugs were injected intradermally into
304 the plantar surface of the hindpaw (20 μL). Radiant heat assays were performed using the IITC
305 Life Science Hargreaves test system. Mechanical threshold was measured using calibrated von
306 Frey monofilaments (Touch Test) on a metal grate platform. Von Frey was performed as
307 previously described[53,54] using the up-down method while blinded to compound injected and
308 genotype. Valid responses for both von Frey and radiant heat included fast paw withdrawal,
309 licking/biting/shaking of the affected paw, or flinching. For radiant heat and von Frey, mice were
310 allowed to acclimate on platform for 1 hour before injection.
311
312 The pinprick assay was conducted on a von Frey testing platform (IITC). The mouse hindpaw
313 was poked with a 31 g syringe needle without breaking the skin to induce fast acute mechanical
314 pain. Each paw was stimulated 10 times with the needle, and the % withdrawal (fast withdrawal,
315 licking/biting/shaking of paw, squeaking, and/or flinching) was calculated from the total number
316 of trials.
317
318 The tape assay was conducted according to previously described methods[6]. Number of
319 attempts to remove a 3 cm piece of lab tape was recorded for 10 minutes after manual tape

320 application to the rostral back. Scorer and experimenter were blinded to genotype.

321

322 For righting reflex measurements, age-matched *S1pr3*$^{-/-}$ and $^{+/+}$ P6-7 neonates were used.
323 Briefly, pups were overturned one at a time on the home cage lid while experimenter was
324 blinded to genotype. The time to righting was measured to the nearest 1/10th of a second with a
325 stopwatch.

326

327 All behavior experiments were carried out using age-matched or littermate cohorts of male mice.
328 Mice were tested in 4-part behavior chambers (IITC Life Sciences) with opaque dividers (TAP
329 Plastics) with the exception of righting reflex measurements. Itch behavior was filmed from
330 below using high-definition cameras. All experiments were performed under the policies and
331 recommendations of the International Association for the Study of Pain and approved by the
332 University of California, Berkeley Animal Care and Use Committee.

333

334 *In situ hybridization (ISH)*

335 Fresh DRG were dissected from 8-12 week old mice, flash frozen in OCT embedding medium,
336 and sectioned at 14 µm onto slides. ISH was performed using Affymetrix Quantigene ViewISH
337 Tissue 2-plex kit according to manufacturer's instructions with Type 1 and Type 6 probes. The
338 following probes against mouse mRNAs were created by Affymetrix and used for ISH: *S1pr3,*
339 *Scn1a,* and *Piezo2.* Slides were mounted in Fluoromount with No. 1.5 coverglass. Imaging of
340 ISH experiments and all other live- and fixed-cell imaging was performed on an Olympus IX71
341 microscope with a Lambda LS-xl light source (Sutter Instruments). Images were analyzed using
342 ImageJ software. Briefly, DAPI-positive cells were circled and their fluorescence intensity (AFU)
343 for all channels was plotted against cell size using Microsoft Excel software. Co-labeling
344 analysis was performed using ImageJ. Intensity thresholds were set based on the negative
345 control (no probe) slide. Cells were defined as co-expressing if their maximum intensities

346 exceeded the threshold for both the Type 1 and Type 6 probe channels.

347

348 *Immunohistochemistry (IHC) of DRG*

349 8-12 week old mice were deeply anesthetized and transcardially perfused with ice-cold PBS
350 followed by ice-cold 4% PFA. DRG were dissected and post-fixed in 4% PFA for one hour. DRG
351 were cryo-protected overnight at 4°C in 30% sucrose-PBS, embedded in OCT, and then
352 sectioned at 12 µm onto slides. Briefly, slides were washed 3x in PBST (0.3% Triton X-100),
353 blocked in 2.5% horse serum + 2.5% BSA PBST, and incubated overnight at 4°C in 1:1000
354 primary antibody in PBST + 0.5% horse serum + 0.5% BSA. Slides were washed 3X in PBS
355 then incubated 1-2 hours at RT in 1:1000 secondary antibody. Slides were washed 3X in PBS
356 and mounted in Fluoromount with No. 1.5 coverglass. Primary antibodies used: Rabbit anti-
357 S1PR3, Mouse anti-NF200, Chicken anti-Peripherin (Abcam). Secondary antibodies used: Goat
358 anti-Mouse Alexa 350, Goat anti-Chicken Alexa 547, Goat anti-Rabbit Alexa 488 (Abcam). Cells
359 labeled with anti-peripherin were circled to define regions of interest.

360

361 *Whole mount skin IHC*

362 Staining was performed according to Marshall and Clary *et al*[55]. Briefly, 8-12 week old mice
363 were euthanized and the back skin was shaved, depilated, and tape-stripped. The removed skin
364 was fixed overnight in 4% PFA, then washed in PBS (3X for 10 minutes each). Dermal fat was
365 scraped away with a scalpel and skin was washed in PBST (0.3% Triton X-100; 3X for two
366 hours each) then incubated in 1:500 primary antibody (Rabbit anti DsRed Polyclonal antibody;
367 Clontech #632496) in blocking buffer (PBST with 5% goat serum and 20% DMSO) for 5.5 days
368 at 4°C. Skin was washed as before and incubated in 1:500 secondary antibody (Goat anti-
369 Rabbit Alexa 594; Invitrogen #R37117) in blocking buffer for 3 days at 4°C. Skin was washed in
370 PBST, serially dried in methanol: PBS solutions, incubated overnight in 100% methanol, and
371 finally cleared with a 1:2 solution of benzyl alcohol: benzyl benzoate (BABB; Sigma) before

372 mounting.

373

374 *Cell culture*

375 Cell culture was carried out as previously described[17]. Briefly, neurons from dorsal root ganglia
376 (2-8 week old adults) or trigeminal ganglia (P0) were dissected and incubated for 10 min in 1.4
377 mg ml−1 Collagenase P (Roche) in Hanks calcium-free balanced salt solution, followed by
378 incubation in 0.25% standard trypsin (vol/vol) STV versene-EDTA solution for 2 min with gentle
379 agitation. Cells were then triturated, plated onto Poly D-Lysine coated glass coverslips and used
380 within 20 h. Media: MEM Eagle's with Earle's BSS medium, supplemented with 10% horse
381 serum (vol/vol), MEM vitamins, penicillin/streptomycin and L-glutamine.

382

383 *Calcium imaging*

384 Ca^{2+} imaging experiments were carried out as previously described[17]. Cells were loaded for 60
385 min at room temperature with 10 μM Fura-2AM supplemented with 0.01% Pluronic F-127
386 (wt/vol, Life Technologies) in a physiological Ringer's solution containing (in mM) 140 NaCl, 5
387 KCl, 10 HEPES, 2 CaCl2, 2 MgCl2 and 10 D-(+)-glucose, pH 7.4. All chemicals were purchased
388 from Sigma. Acquired images were displayed as the ratio of 340 nm/ 380 nm. Cells were
389 identified as neurons by eliciting depolarization with high potassium Ringer's solution (75 mM) at
390 the end of each experiment. Responding neurons were defined as those having a > 15%
391 increase from baseline ratio. Image analysis and statistics were performed using automated
392 routines in Igor Pro (WaveMetrics). Fura-2 ratios were normalized to the baseline ratio
393 F340/F380 = (Ratio)/(Ratio t = 0).

394

395 *Ex vivo skin-nerve electrophysiology*

396 Touch-evoked responses in the skin were recorded after dissecting the hind limb skin and
397 saphenous nerve from 7-10 week old mice, according to published methods[56,57]. The skin was

398 placed epidermis-side-up in a custom chamber and perfused with carbogen-buffered synthetic
399 interstitial fluid (SIF) kept at 32 °C with a temperature controller (model TC-344B, Warner
400 Instruments). The nerve was kept in mineral oil in a recording chamber, teased apart, and
401 placed onto a gold recording electrode connected with a reference electrode to a differential
402 amplifier (model 1800, A-M Systems). The extracellular signal was digitized using a PowerLab
403 8/35 board (AD Instruments) and recorded using LabChart software (AD Instruments).
404
405 For these studies, we focused on A-mechanonociceptors (AMs). To identify responses from
406 these afferents in mutant and control genotypes, we used a mechanical search paradigm with a
407 fine glass probe. Afferents were classified as AMs according to the following criteria: (1) Aδ
408 conduction velocity (approximately, 1 to (≤ 12 m/s^{-1}), (2) medium-sized receptive fields, (3)
409 sustained response to mechanical indentation[9,57,58].
410
411 Touch-sensitive afferents that did not meet these criteria were not analyzed further. Responses
412 were classified as Adapting AMs if the ratio of mean firing rate in the dynamic phase of
413 stimulation (first 0.2 s) to the static phase of stimulation (last 4.8 s) was greater than 2, and Non-
414 Adapting AMs if the ratio was less than or equal to 2. Non-responders (Fig. 4g) responded to
415 suprathreshold mechanical stimulation with von Frey monofilaments (tip diameter <0.5 mm), but
416 not to maximal controlled mechanical stimulation (256 mN, tip diameter 2 mm). All recordings
417 and analyses were performed blind to genotype.
418
419 Mechanical responses were elicited with von Frey monofilaments and a force controlled custom-
420 built mechanical stimulator. Mechanical thresholds were defined as the lowest von Frey
421 monofilament to reliable elicit at least on action potential. Force controlled mechanical stimuli
422 were delivered using a computer controlled, closed-loop, mechanical stimulator (Model 300C-I,
423 Aurora Scientific, 2 mm tip diameter). Low-pass filtered, 5-second long, length control steps

424 (square wave) simultaneously delivered with permissive force control steps (square wave) were
425 generated using LabChart software (AD Instruments). An arbitrarily selected force step-and-hold
426 protocol (8, 32, 4, 64, 128, 16, 256 mN) was delivered to all fibers. The period between
427 successive displacements was 60 seconds.
428
429 Conduction velocity was measured by electrically stimulating identified receptive fields. Spike
430 sorting by principal component analysis (PCA) and density based clustering, and data analysis
431 was performed off-line with custom-made software in MATLAB. Statistics were performed in
432 Prism.
433
434 *In vitro electrophysiology*
435 Electrophysiological experiments were carried out as previously described[17]. Briefly, recordings
436 were collected at 5 kHz and filtered at 2 kHz (Axopatch 200B, pClamp software). Electrode
437 resistance ranged between 1.5–5 MΩ. Internal solution contained 140 mM KCl, 2 mM MgCl2, 1
438 mM EGTA, 5 mM HEPES, 1 mM Na2ATP, 100 μM GTP, and 100 μM cAMP (pH 7.4). Bath
439 solution was physiological Ringer's solution. The pipette potential was canceled before seal
440 formation. Cell capacitance was canceled before whole cell voltage-clamp recordings.
441 Experiments were carried out only on cells with a series resistance of less than 30 MΩ. Analysis
442 of electrophysiology data was performed in pClamp and IgorPro.
443
444 *Statistical analyses*
445 All statistical analyses, except for skin nerve data (see above), were performed using IgorPro
446 software or Microsoft Excel. Values are reported as the mean ± SEOM where multiple
447 independent experiments are pooled and reported (for whole cell electrophysiology), and mean
448 ± SD where one experiment was performed with multiple wells (for calcium imaging) or mice (for
449 behavior). For comparison between two groups, Student's unpaired 2-tailed t-test was used. A

450 paired t-test was employed only for measurements within the same biological replicate and after
451 a given treatment. For single-point comparison between >2 groups, a one-way ANOVA followed
452 by Tukey Kramer post hoc test was used. For the time course comparison between 2 groups, 2-
453 way ANOVA was used and single comparison p-values were derived using Tukey's HSD. For
454 comparing distributions, a type II Kolmogorov-Smirnov test was used. Number of mice or
455 samples required to attain significance was not calculated beforehand, and where multiple
456 statistical tests were performed, a Bonferroni correction was applied. In figure legends,
457 significance was labeled as: n.s., not significant, $p \geq 0.05$; *$p < 0.05$; **$p < 0.01$; ***$p < 0.001$.
458

459 Author Contributions

460 R.Z.H, D.M.B., and R.B. conceived experiments and wrote the manuscript. R.Z.H. performed
461 behavioral, immunostaining, whole cell electrophysiology, calcium imaging, and ISH, and
462 analyzed data and made figures. T.M. also performed ISH experiments. E. A. L. & B.H.
463 conceived and analyzed *ex vivo* recordings. B.U.H. and S. C. performed *ex vivo* recordings. All
464 authors contributed to the final version of the manuscript.
465

466 Acknowledgements

467 We thank Z. Rifi (UC Berkeley) for assistance with scoring itch behavior, R. P. Dalton (UC
468 Berkeley) for assistance with confocal microscopy, and P. Lishko and M. Miller (UC Berkeley)
469 for advice regarding lipid stability and usage. We would also like to thank R. Clary (Columbia)
470 for whole mount skin staining protocols and D. Julius (UC San Francisco) for the gift of Hm1a
471 spider toxin. We are grateful to all members of the D.M.B Laboratory (UC Berkeley) for
472 constructive feedback and criticism. The National Institutes of Health grants NS077224 (to
473 D.M.B and R.B.), AR059385 (to D.M.B.), AR051219 (to E.A.L), NS105449 and GM007367 (to
474 B.U.H), and NS063307 (to the Neurobiology Course at the Marine Biological Laboratory); and a

475 Howard Hughes Medical Institute Faculty Scholars grant (to D.M.B) supported this work.

476 ## Competing interests

477 The authors declare no competing interests at this time.

478

479 ## References

480 1. Caterina, M. J., Schumacher, M. a, Tominaga, M., Rosen, T. a, Levine, J. D. & Julius, D.
481 The capsaicin receptor: a heat-activated ion channel in the pain pathway. *Nature* **389,**
482 816–824 (1997).

483 2. Caterina, M. J, Leffler. A., Malmberg, A. B., Martin, W. J., Trafton, J., Petersen-Zeitz, K.
484 R., Koltzenburg, M., Basbaum, A. I., Julius, J. D. Impaired Nociception and Pain
485 Sensation in Mice Lacking the Capsaicin Receptor. *Science* **288,** 306–313 (2000).

486 3. McKemy, D. D., Neuhausser, W. M. & Julius, D. Identification of a cold receptor reveals a
487 general role for TRP channels in thermosensation. *Nature* **416,** 52–58 (2002).

488 4. Bautista, D. M., Siemens, J., Glazer, J. M., Tsuruda, P. R., Basbaum, A. I., Stucky, C. L.,
489 Jordt, S.-E. & Julius, D. The menthol receptor TRPM8 is the principal detector of
490 environmental cold. *Nature* **448,** 204–208 (2007).

491 5. Coste, B., Mathur, J., Schmidt, M., Earley, T. J., Ranade, S., Petrus, M. J., Dubin, A. E. &
492 Patapoutian, A. Piezo1 and Piezo2 Are Essential Components of Distinct Mechanically
493 Activated Cation Channels. *Science* **330,** 55–60 (2010).

494 6. Ranade, S. S., Woo, S., Dubin, A. E., Moshourab, R. a, Wetzel, C., Petrus, M., Mathur,
495 J., Bégay, V., Coste, B., Mainquist, J., Wilson, a J., Francisco, A. G., Reddy, K., Qiu, Z.,
496 Wood, N., Lewin, G. R. & Patapoutian, A. Piezo2 is the major transducer of mechanical
497 forces for touch sensation in mice. *Nature* **516,** 121–125 (2014).

498 7. Woo, S.-H., Ranade, S., Weyer, A. D., Dubin, A. E., Baba, Y., Qiu, Z., Petrus, M.,
499 Miyamoto, T., Reddy, K., Lumpkin, E. a., Stucky, C. L. & Patapoutian, A. Piezo2 is
500 required for Merkel-cell mechanotransduction. *Nature* **509,** 622–626 (2014).

501 8. Basbaum, A. I., Bautista, D. M., Scherrer, G. & Julius, D. Cellular and Molecular
502 Mechanisms of Pain. *Cell* **139,** 267–284 (2009).
503 9. Koltzenburg, M., Stucky, C. L., Lewin, G. R., Bautista, M., Lechner, S. G., Gemes, G.,
504 Koopmeiners, A., Rigaud, M., Lirk, P., Sapunar, D., Latha, M., Vilceanu, D., Garrison, S.
505 R., Ljubkovic, M., Mueller, S. J., Cheryl, L. & Hogan, Q. H. Receptive Properties of Mouse
506 Sensory Neurons Innervating Hairy Skin Receptive Properties of Mouse Sensory
507 Neurons Innervating Hairy Skin. *J. Neurophysiol.* **78,** 1841–1850 (1997).
508 10. Osteen, J. D., Herzig, V., Gilchrist, J., Emrick, J. J., Zhang, C., Wang, X., Castro, J.,
509 Garcia-Caraballo, S., Grundy, L., Rychkov, G. Y., Weyer, A. D., Dekan, Z., Undheim, E.
510 A. B., Alewood, P., Stucky, C. L., Brierley, S. M., Basbaum, A. I., Bosmans, F., King, G.
511 F. & Julius, D. Selective spider toxins reveal a role for the Nav1.1 channel in mechanical
512 pain. *Nature* **534,** 494–9 (2016).
513 11. Arcourt, A., Gorham, L., Dhandapani, R., Prato, V., Taberner, F. J., Wende, H.,
514 Gangadharan, V., Birchmeier, C., Heppenstall, P. A. & Lechner, S. G. Touch Receptor-
515 Derived Sensory Information Alleviates Acute Pain Signaling and Fine-Tunes Nociceptive
516 Reflex Coordination. *Neuron* **93,** 179–193 (2017).
517 12. Ghitani, N., Barik, A., Szczot, M., Thompson, J. H., Li, C., Le Pichon, C. E., Krashes, M.
518 J. & Chesler, A. T. Specialized Mechanosensory Nociceptors Mediating Rapid
519 Responses to Hair Pull. *Neuron* **95,** 944–954.e4 (2017).
520 13. Duan, B., Cheng, L., Bourane, S., Britz, O., Padilla, C., Garcia-campmany, L., Krashes,
521 M., Knowlton, W., Velasquez, T., Ren, X., Ross, S. E., Lowell, B. B., Wang, Y., Goulding,
522 M. & Ma, Q. Identification of Spinal Circuits Transmitting and Gating Mechanical Pain.
523 *Cell* **159,** 1417–1432 (2014).
524 14. Gerhold, K. a., Pellegrino, M., Tsunozaki, M., Morita, T., Leitch, D. B., Tsuruda, P. R.,
525 Brem, R. B., Catania, K. C. & Bautista, D. M. The Star-Nosed Mole Reveals Clues to the
526 Molecular Basis of Mammalian Touch. *PLoS One* **8,** (2013).

527 15. Usoskin, D., Furlan, A., Islam, S., Abdo, H., Lönnerberg, P., Lou, D., Hjerling-Leffler, J.,
528 Haeggström, J., Kharchenko, O., Kharchenko, P. V, Linnarsson, S. & Ernfors, P.
529 Unbiased classification of sensory neuron types by large-scale single-cell RNA
530 sequencing. *Nat. Neurosci.* **18,** 145–153 (2015).
531 16. Kono, M., Mi, Y., Liu, Y., Sasaki, T., Allende, M. L., Wu, Y. P., Yamashita, T. & Proia, R.
532 L. The sphingosine-1-phosphate receptors S1P1, S1P2, and S1P3 function coordinately
533 during embryonic angiogenesis. *J. Biol. Chem.* **279,** 29367–29373 (2004).
534 17. Wilson, S. R., Gerhold, K. a, Bifolck-Fisher, A., Liu, Q., Patel, K. N., Dong, X. & Bautista,
535 D. M. TRPA1 is required for histamine-independent, Mas-related G protein-coupled
536 receptor-mediated itch. *Nat. Neurosci.* **14,** 595–602 (2011).
537 18. Chiba, Y., Takeuchi, H., Sakai, H. & Misawa, M. SKI-II, an inhibitor of sphingosine kinase,
538 ameliorates antigen-induced bronchial smooth muscle hyperresponsiveness, but not
539 airway inflammation, in mice. *J. Pharmacol. Sci.* **114,** 304–310 (2010).
540 19. Mair, N., Benetti, C., Andratsch, M., Leitner, M. G., Constantin, C. E., Camprubí-Robles,
541 M., Quarta, S., Biasio, W., Kuner, R., Gibbins, I. L., Kress, M. & Haberberger, R. V.
542 Genetic evidence for involvement of neuronally expressed s1P1 receptor in nociceptor
543 sensitization and inflammatory pain. *PLoS One* **6,** (2011).
544 20. Shaner, R. L., Allegood, J. C., Park, H., Wang, E., Kelly, S., Haynes, C. a, Sullards, M. C.
545 & Merrill, A. H. Quantitative analysis of sphingolipids for lipidomics using triple quadrupole
546 and quadrupole linear ion trap mass spectrometers. *J. Lipid Res.* **50,** 1692–1707 (2009).
547 21. Camprubi-Robles, M., Mair, N., Andratsch, M., Benetti, C., Beroukas, D., Rukwied, R.,
548 Langeslag, M., Proia, R. L., Schmelz, M., Ferrer Montiel, A. V, Haberberger, R. V, Kress,
549 M. & Camprubí-Robles, M. Sphingosine-1-phosphate-induced nociceptor excitation and
550 ongoing pain behavior in mice and humans is largely mediated by S1P3 receptor. *J.*
551 *Neurosci.* **33,** 2582–2592 (2013).
552 22. Abrahamsen, B., Zhao, J., Asante, C. O., Cendan, C. M., Marsh, S., Martinez-Barbera, J.

553 P., Nassar, M. A., Dickenson, A. H. & Wood, J. N. The Cell and Molecular Basis of
554 Mechanical, Cold, and Inflamatory Pain. *Science* **321,** 702 (2008).
555 23. Sanna, M. G., Vincent, K. P., Repetto, E., Nhan, N., Brown, S. J., Abgaryan, L., Riley, S.
556 W., Leaf, N. B., Cahalan, S. M., Kiosses, W. B., Kohno, Y., Heller Brown, J., McCulloch,
557 A. D., Rosen, H. & Gonzalez-Cabrera, P. J. Bitopic S1P3 Antagonist Rescue from
558 Complete Heart Block: Pharmacological and Genetic Evidence for Direct S1P3
559 Regulation of Mouse Cardiac Conduction. *Mol. Pharmacol.* **89,** 176–186 (2015).
560 24. Schu, S., Orozco, I. J. & Jentsch, T. J. KCNQ Potassium Channels Modulate Sensitivity
561 of Skin Down hair (D-hair) Mechanoreceptors. *J. Biol. Chem.* **291,** 5566–5575 (2016).
562 25. Zheng, Q., Fang, D., Liu, M., Cai, J., Wan, Y., Han, J. S. & Xing, G. G. Suppression of
563 KCNQ/M (Kv7) potassium channels in dorsal root ganglion neurons contributes to the
564 development of bone cancer pain in a rat model. *Pain* **154,** 434–448 (2013).
565 26. Crozier, R. A., Ajit, S. K., Kaftan, E. J. & Pausch, M. H. MrgD Activation Inhibits KCNQ /
566 M-Currents and Contributes to Enhanced Neuronal Excitability. *J. Neurosci.* **27,** 4492–
567 4496 (2007).
568 27. Heidenreich, M., Lechner, S. G., Vardanyan, V., Wetzel, C., Cremers, C. W., De
569 Leenheer, E. M., Aránguez, G., Moreno-Pelayo, M. Á., Jentsch, T. J. & Lewin, G. R.
570 KCNQ4 K(+) channels tune mechanoreceptors for normal touch sensation in mouse and
571 man. *Nat. Neurosci.* **15,** 138–145 (2012).
572 28. Bäumer, W., Rossbach, K., Mischke, R., Reines, I., Langbein-Detsch, I., Lüth, A. &
573 Kleuser, B. Decreased concentration and enhanced metabolism of sphingosine-1-
574 phosphate in lesional skin of dogs with atopic dermatitis: disturbed sphingosine-1-
575 phosphate homeostasis in atopic dermatitis. *J. Invest. Dermatol.* **131,** 266–268 (2011).
576 29. Ramos-Perez, W. D., Fang, V., Escalante-Alcalde, D., Cammer, M. & Schwab, S. R. A
577 map of the distribution of sphingosine 1-phosphate in the spleen. *Nat. Immunol.* **16,**
578 1245–52 (2015).

579 30. Suh, B.-C., Inoue, T., Meyer, T. & Hille, B. Rapid Chemically Induced Changes of
580 PtdIns(4,5)P2 Gate KCNQ Ion Channels. *Science* **314,** 1454–1457 (2006).
581 31. Blackburn-Munro, G. & Jensen, B. S. The anticonvulsant retigabine attenuates
582 nociceptive behaviours in rat models of persistent and neuropathic pain. *Eur. J.*
583 *Pharmacol.* **460,** 109–116 (2003).
584 32. Hayashi, H., Iwata, M., Tsuchimori, N. & Matsumoto, T. Activation of peripheral KCNQ
585 channels attenuates inflammatory pain. *Mol. Pain* **10,** 15 (2014).
586 33. Matloubian, M., Lo, C. G., Cinamon, G., Lesneski, M. J., Xu, Y., Brinkmann, V., Allende,
587 M. L., Proia, R. L. & Cyster, J. G. Lymphocyte egress from thymus and peripheral
588 lymphoid organs is dependent on S1P receptor 1. *Nature* **427,** 355–360 (2004).
589 34. Pinho-Ribeiro, F. A., Verri, W. A. & Chiu, I. M. Nociceptor Sensory Neuron–Immune
590 Interactions in Pain and Inflammation. *Trends Immunol.* **38,** 5–19 (2017).
591 35. Oetjen, L. K., Mack, M. R., Feng, J., Whelan, T. M., Niu, H., Guo, C. J., Chen, S., Trier, A.
592 M., Xu, A. Z., Tripathi, S. V., Luo, J., Gao, X., Yang, L., Hamilton, S. L., Wang, P. L.,
593 Brestoff, J. R., Council, M. L., Brasington, R., Schaffer, A., Brombacher, F., Hsieh, C.-S.,
594 Gereau, R. W., Miller, M. J., Chen, Z.-F., Hu, H., Davidson, S., Liu, Q. & Kim, B. S.
595 Sensory Neurons Co-opt Classical Immune Signaling Pathways to Mediate Chronic Itch.
596 *Cell* **129,** 742–751 (2017).
597 36. Donoviel, M. S., Hait, N. C., Ramachandran, S., Maceyka, M., Takabe, K., Milstien, S.,
598 Oravecz, T. & Spiegel, S. Spinster 2, a sphingosine 1-phosphate transporter, plays a
599 Critical Role in inflammatory and Autoimmune Diseases. *FASEB J.* **29,** 5018–5028
600 (2015).
601 37. Schwab, S. R., Pereira, J. P., Matloubian, M., Xu, Y., Huang, Y. & Cyster, J. G.
602 Lymphocyte sequestration through S1P lyase inhibition and disruption of S1P gradients.
603 *Science* **309,** 1735–1739 (2005).
604 38. Allende, M. L., Bektas, M., Lee, B. G., Bonifacino, E., Kang, J., Tuymetova, G., Chen, W.,

605 Saba, J. D. & Proia, R. L. Sphingosine-1-phosphate lyase deficiency produces a pro-
606 inflammatory response while impairing neutrophil trafficking. *J. Biol. Chem.* **286,** 7348–
607 7358 (2011).
608 39. Weth-Malsch, D., Langeslag, M., Beroukas, D., Zangrandi, L., Kastenberger, I., Quarta,
609 S., Malsch, P., Kalpachidou, T., Schwarzer, C., Proia, R. L., Haberberger, R. V. & Kress,
610 M. Ablation of Sphingosine 1-Phosphate Receptor Subtype 3 Impairs Hippocampal
611 Neuron Excitability In vitro and Spatial Working Memory In vivo. *Front. Cell. Neurosci.* **10,**
612 1–12 (2016).
613 40. Mitroi, D. N., Deutschmann, A. U., Raucamp, M., Karunakaran, I., Glebov, K., Hans, M.,
614 Walter, J., Saba, J., Gräler, M., Ehninger, D., Sopova, E., Shupliakov, O., Swandulla, D.
615 & van Echten-Deckert, G. Sphingosine 1-phosphate lyase ablation disrupts presynaptic
616 architecture and function via an ubiquitin- proteasome mediated mechanism. *Sci. Rep.* **6,**
617 37064 (2016).
618 41. Chan, J. P. & Sieburth, D. Localized Sphingolipid Signaling at Presynaptic Terminals Is
619 Regulated by Calcium Influx and Promotes Recruitment of Priming Factors. *J. Neurosci.*
620 **32,** 17909–17920 (2012).
621 42. Riganti, L., Antonucci, F., Gabrielli, M., Prada, I., Giussani, P., Viani, P., Valtorta, F.,
622 Menna, E., Matteoli, M. & Verderio, C. Sphingosine-1-Phosphate (S1P) Impacts
623 Presynaptic Functions by Regulating Synapsin I Localization in the Presynaptic
624 Compartment. *J. Neurosci.* **36,** 4624–4634 (2016).
625 43. Choi, J. W., Gardell, S. E., Herr, D. R., Rivera, R., Lee, C.-W., Noguchi, K., Teo, S. T.,
626 Yung, Y. C., Lu, M., Kennedy, G. & Chun, J. FTY720 (fingolimod) efficacy in an animal
627 model of multiple sclerosis requires astrocyte sphingosine 1-phosphate receptor 1 (S1P1)
628 modulation. *Proc. Natl. Acad. Sci. U. S. A.* **108,** 751–6 (2011).
629 44. Di Pardo, A., Amico, E., Favellato, M., Castrataro, R., Fucile, S., Squitieri, F. & Maglione,
630 V. FTY720 (fingolimod) is a neuroprotective and disease-modifying agent in cellular and

631 mouse models of huntington disease. *Hum. Mol. Genet.* **23,** 2251–2265 (2014).

632 45. Zhao, P., Yang, X., Yang, L., Li, M., Wood, K., Liu, Q. & Zhu, X. Neuroprotective effects
633 of fingolimod in mouse models of Parkinson's disease. *FASEB J.* **31,** 172–179 (2017).

634 46. Couttas, T. a, Kain, N., Daniels, B., Lim, X. Y., Shepherd, C., Kril, J., Pickford, R., Li, H.,
635 Garner, B. & Don, A. S. Loss of the neuroprotective factor Sphingosine 1-phosphate early
636 in Alzheimer's disease pathogenesis. *Acta Neuropathol. Commun.* **2,** 9 (2014).

637 47. Nomura, T., Cranfield, C. G., Deplazes, E., Owen, D. M., Macmillan, a., Battle, a. R.,
638 Constantine, M., Sokabe, M. & Martinac, B. Differential effects of lipids and lyso-lipids on
639 the mechanosensitivity of the mechanosensitive channels MscL and MscS. *Proc. Natl.*
640 *Acad. Sci.* **109,** 8770–8775 (2012).

641 48. Brohawn, S. G., Su, Z. & MacKinnon, R. Mechanosensitivity is mediated directly by the
642 lipid membrane in TRAAK and TREK1 K+ channels. *Proc. Natl. Acad. Sci. U. S. A.* **111,**
643 3614–9 (2014).

644 49. Scholz, N., Guan, C., Nieberler, M., Grotemeyer, A., Maiellaro, I., Gao, S., Beck, S.,
645 Pawlak, M., Sauer, M., Asan, E., Rothemund, S., Winkler, J., Prömel, S., Nagel, G.,
646 Langenhan, T. & Kittel, R. J. Mechano-dependent signaling by Latrophilin/CIRL quenches
647 cAMP in proprioceptive neurons. *Elife* **6,** 1–21 (2017).

648 50. Morita, T., McClain, S. P., Batia, L. M., Pellegrino, M., Wilson, S. R., Kienzler, M. A.,
649 Lyman, K., Olsen, A. S. B., Wong, J. F., Stucky, C. L., Brem, R. B. & Bautista, D. M.
650 HTR7 Mediates Serotonergic Acute and Chronic Itch. *Neuron* **87,** 124–138 (2015).

651 51. Tsunozaki, M., Lennertz, R. C., Vilceanu, D., Katta, S., Stucky, C. L. & Bautista, D. M. A
652 'toothache tree' alkylamide inhibits Aδ mechanonociceptors to alleviate mechanical pain.
653 *J. Physiol.* **591,** 3325–40 (2013).

654 52. Shimada, S. G. & LaMotte, R. H. Behavioral differentiation between itch and pain in
655 mouse. *Pain* **139,** 681–687 (2008).

656 53. Dixon, W. J. The Up-and-Down Method for Small Samples. *J. Am. Stat. Assoc.* **60,** 967–

657 978 (1980).

658 54. Chaplan, SR, Bach, FW, Pogrel, JW, Chung, JM, Yaksh, T. Quantitative assessment of
659 tactile allodynia evoked by unilateral ligation of the fifth and sixth lumbar nerves in the rat.
660 *J. Neurosci.* **53,** 55–63 (1994).

661 55. Marshall, K. L., Clary, R. C., Baba, Y., Orlowsky, R. L., Gerling, G. J. & Lumpkin, E. A.
662 Touch Receptors Undergo Rapid Remodeling in Healthy Skin. *Cell Rep.* **17,** 1719–1727
663 (2016).

664 56. Maksimovic, S., Nakatani, M., Baba, Y., Nelson, A. M., Marshall, K. L., Wellnitz, S. A.,
665 Firozi, P., Woo, S.-H., Ranade, S., Patapoutian, A. & Lumpkin, E. A. Epidermal Merkel
666 cells are mechanosensory cells that tune mammalian touch receptors. *Nature* **509,** 617–
667 621 (2014).

668 57. Wellnitz, S. A., Lesniak, D. R., Gerling, G. J. & Lumpkin, E. A. The Regularity of
669 Sustained Firing Reveals Two Populations of Slowly Adapting Touch Receptors in Mouse
670 Hairy Skin. *J. Neurophysiol.* **103,** 3378–3388 (2010).

671 58. Zimmermann, K., Hein, A., Hager, U., Kaczmarek, J. S., Turnquist, B. P., Clapham, D. E.
672 & Reeh, P. W. Phenotyping sensory nerve endings in vitro in the mouse. *Nat. Protoc.* **4,**
673 (2009).

674

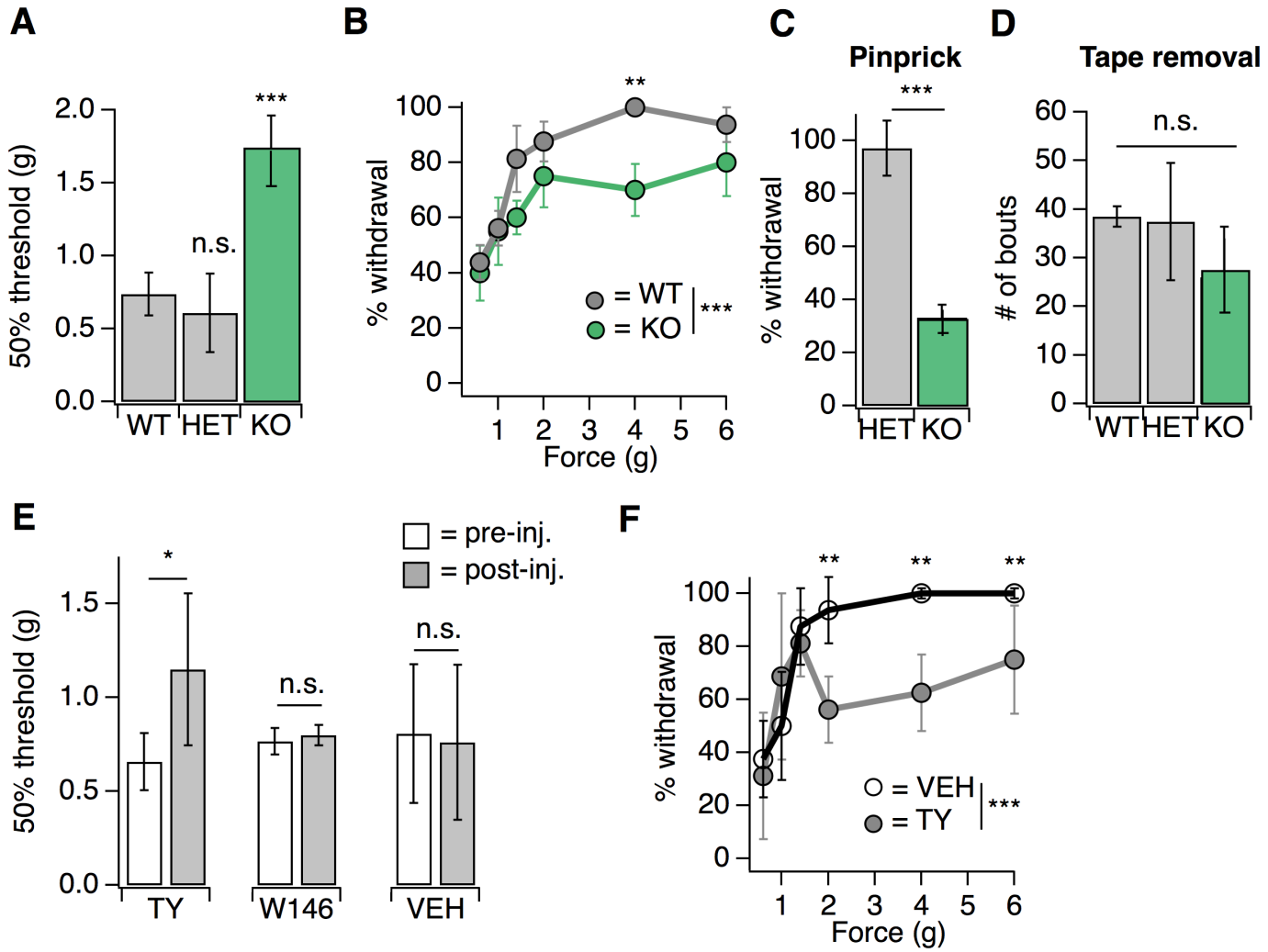

Figure 1. S1PR3 mediates acute mechanical pain. A. von Frey 50% withdrawal threshold measurements for *S1pr3*$^{+/+}$ (WT, N = 8), $^{+/-}$ (HET, N = 7) and $^{-/-}$ (KO, N = 12) mice. $p < 0.0001$ (one-way ANOVA). Tukey Kramer post hoc comparisons for KO and HET to WT indicated on graph. B. von Frey force-response graph for WT (N = 8) versus KO (N = 12) animals; $p_{genotype} < 0.0001$ (two-way ANOVA). Tukey HSD comparisons between genotypes are indicated for given forces. C. % withdrawal to pinprick stimulation of hindpaw for HET versus KO animals; $p < 0.0001$ (unpaired t-test; N = 5-7 mice per group). D. Number of attempted removal bouts in tape assay for WT (N =2), HET (N = 2), and KO (N = 5) mice; $p = 0.172$ (one-way ANOVA). E. von Frey 50% withdrawal threshold measurements for mice pre- and post-injection of 500 μM TY 52156 (N = 10), 10 μM W146 (N = 6), or 1% DMSO-PBS vehicle (N = 17); $p = 0.016$, 0.650 (two-tailed paired t-test comparing vehicle- vs. drug-injected paw). F. von Frey force-response graph for mice injected with either 1% DMSO-PBS or 500 μM TY 52156; $p_{treatment} < 1e\text{-}05$ (two-way ANOVA; N = 4 mice per group). Tukey HSD comparisons were made between treatment groups and significant differences at a given force are indicated on graph. Unless otherwise indicated, error bars represent mean ± SD. See Source Data Table 1 for additional details.

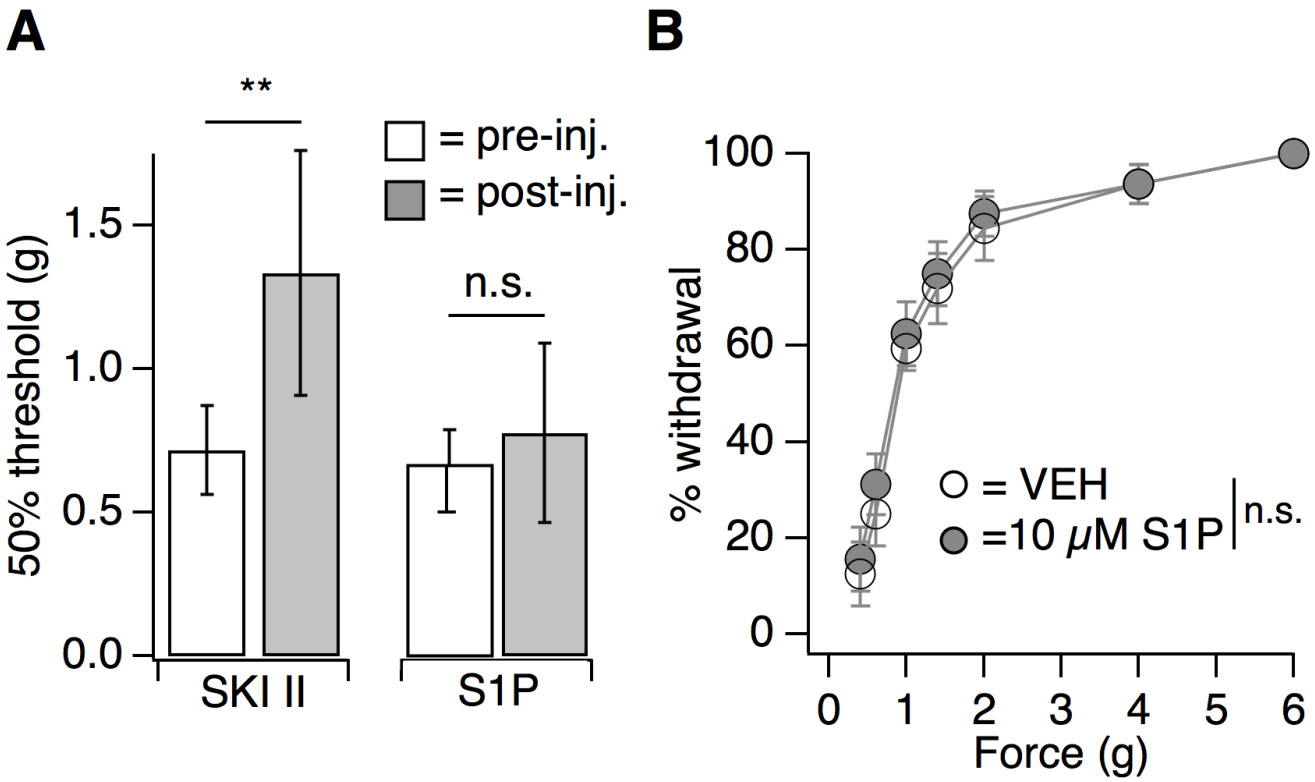

Figure 2. Endogenous S1P mediates acute mechanical pain. A. von Frey 50% withdrawal measurements for mice pre- and post-injection of 50 μM SKI II (N = 8) or 10 μM S1P (N = 7); p = 0.003, 0.604 (two-tailed paired t-test). B. von Frey force-response graph for animals injected with 10 μM S1P or 0.1% MeOH-PBS; $p_{genotype}$ > 0.05 (two-way ANOVA; N = 8 mice per group). No Tukey HSD comparisons at any force between genotypes were significant. Error bars represent mean ± SD. See Source Data Table 2 for additional details.

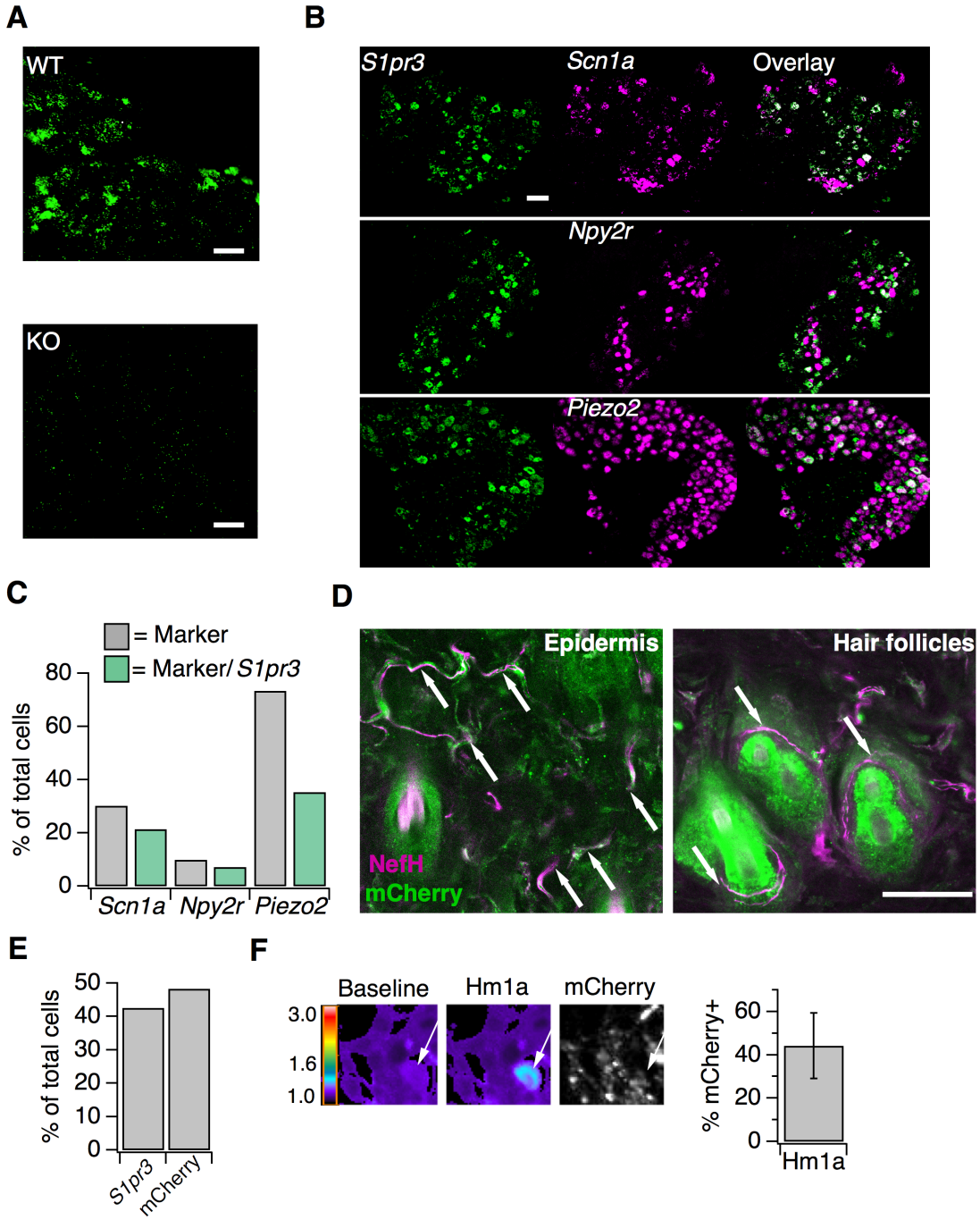

Figure 3. S1PR3 is expressed in A mechanonociceptors. A. ISH of *S1pr3* (green) in sectioned DRG from adult wild-type (top) and S1PR3 KO (bottom) mice (20x air objective; scale = 50 µm). B. Representative Co-ISH of *S1pr3* (green; left) with *Scn1a*, *Npy2r,* and *Piezo2* (magenta; center). Right column: overlay with co-localized regions colored white (10x air objective; scale = 100 µm). C. Bar chart showing the % of total cells expressing the indicated marker (grey) and the % of total cells co-expressing both marker and *S1pr3* (green) from the images in Fig. 3B. D. Whole-mount skin immunohistochemistry with anti-DsRed antibody (green) and anti-NefH antibody (magenta) in an *S1pr3*$^{mCherry/+}$ animal (20x water objective; scale = 50 µm). Arrows indicate S1PR3+ epidermal fibers (left image) or S1PR3- circumferential fibers (right image). E. Quantification of % of total cells expressing *S1pr3* from DRG ISH and mCherry from dissociated DRG cultures (N = 2 animals each experiment). F. (Left) Fura-2 AM calcium imaging before (left) and after (center) addition of 500 nM Hm1a in *S1pr3*$^{mCherry/+}$ P0 TG neurons. Right-hand image indicates mCherry fluorescence. Arrows indicate one mCherry+/Hm1a-responsive cell. (Right) % of Hm1a-responsive P0 TG neurons that are mCherry+ (N = 1 animal, 1230 total neurons).

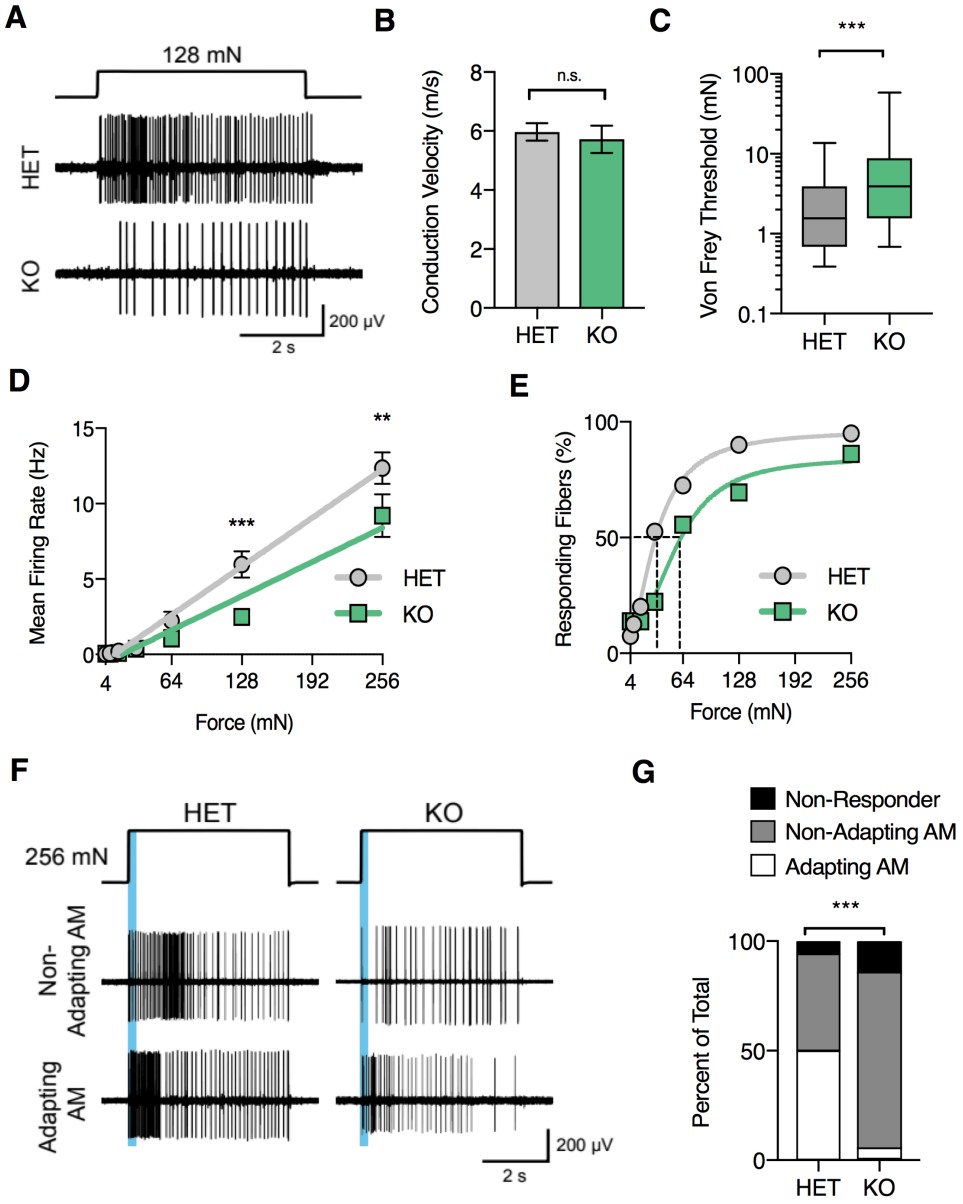

Figure 4. S1PR3 is required for nociceptive responses of high-threshold AM nociceptors. A. Representative traces of AM fiber activity over time in *ex vivo* skin-saphenous nerve recording in response to stimulation (128 mN, top) from S1PR3$^{+/-}$ (HET) (middle) and $^{-/-}$ (KO) (bottom) mice. B. Conduction velocity (CV) of AM fibers in S1PR3 HET and KO mice. p = 0.65 (two-tailed t-test); N = 40, 36 fibers; errors, mean ± SEM. C. von Frey threshold of AM fibers in S1PR3 HET and KO skin. ***p < 0.0001 (Mann-Whitney test); lines, median; boxes, 25-75 percentile; whiskers, min-max. D. Mean firing rate of AM fibers in response to force controlled stimulation (4,8,16,32,64,128,256 mN). **p=0.001, ***p=0.0002 (two-way ANOVA, Sidak's post-hoc); lines, linear regression (HET: slope, 50 Hz/N, R^2, 0.99; KO: slope, 35 Hz/N, R^2, 0.95). E. Cumulative response plot of AM fibers to force controlled stimulation (solid lines); four-parameter logistic fit from which half-maximal force was estimated for each genotype (dotted lines). F. Representative traces of Non-Adapting and Adapting AMs in response to force controlled stimulation (256 mN, top) for S1PR3 HET and KO mice; blue regions, dynamic phase of stimulation. G. Proportion of fibers classified by pattern of mechanically evoked responses to 256 mN of stimulation: Non-Responder (HET, 2/40 fibers; KO 5/36), Non-Adapting AM (HET, 18/40; KO, 29/36), Adapting AM (HET, 20/40; KO, 2/36). Non-Responders fired action potentials to large magnitude von Frey monofilaments (<0.5 mm tip diameter), but not to 256 mN of controlled mechanical stimulation (2 mm tip diameter). Classification of Non-Adapting vs. Adapting AMs detailed in methods. ***p<0.00001 (Chi-square test). See Source Data Table 4 for additional details.

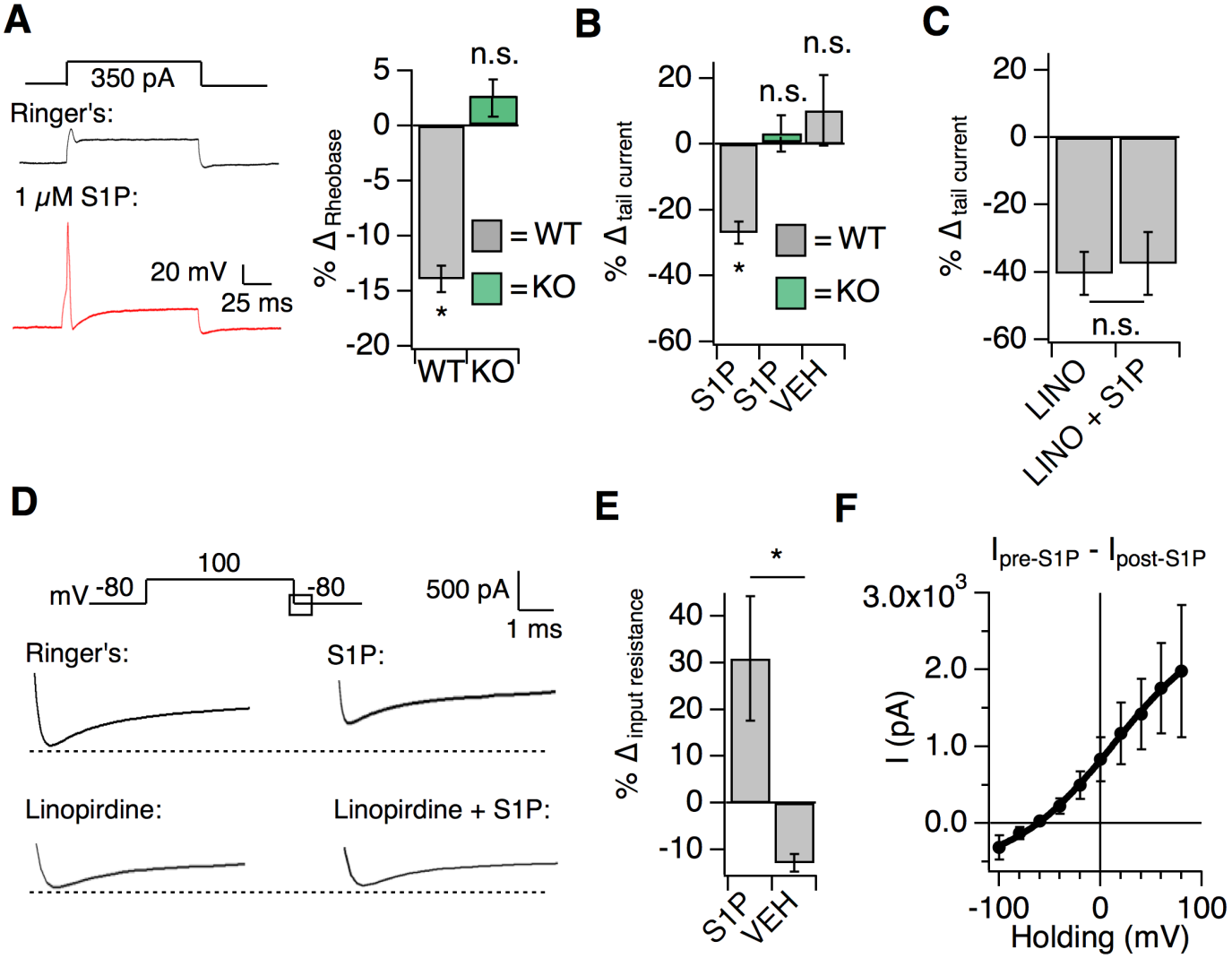

Figure 5. S1PR3 modulates KCNQ2/3 channels to regulate AM excitability. All experiments were performed in *S1pr3*$^{mCherry/+}$ or $^{-/-}$ DRG neurons. A. (Left) Example traces of a single mCherry+ neuron in whole cell current clamp before and after S1P application. (Right) % change in rheobase after S1P application for *S1pr3*$^{mCherry/+}$ (left) and KO (right) neurons ($p_{WT,KO}$ = 0.012, 0.287; two-tailed paired t-test; N = 7, 12 cells). B. % Δ in tail current after S1P or 1% DMSO vehicle application for *S1pr3*$^{mCherry/+}$ and KO medium-diameter neurons (p = 0.014; one-way ANOVA; N = 10, 13, 10 cells). Tukey Kramer post hoc *p*-values indicated on graph. C. % Δ in tail current after indicated treatments (LINO = 100 μM linopirdine) for *S1pr3*$^{mCherry/+}$ medium-diameter neurons; (p = 0.47; two-tailed paired t-test; N = 12 cells). D. (Top) Averaged tail current traces of a single mCherry+ neuron in whole cell voltage clamp recording pre- and post-S1P. (Bottom) Averaged tail current traces of a single mCherry+ neuron in whole cell voltage clamp recording with indicated treatment. E. % Δ in input resistance after S1P or vehicle application (p = 0.017; two-tailed paired t-test; N = 4 cells per group). F. Instantaneous current-voltage relationship after subtraction of the post-S1P current from the pre-S1P current. Current reverses at -60.125 mV; N = 6 cells. Data were fitted with a Boltzmann equation. A pre-pulse stimulation of +100 mV for 100 ms was used. Unless indicated otherwise, all error bars represent mean ± SEOM. See Source Data Table 5 for additional details.

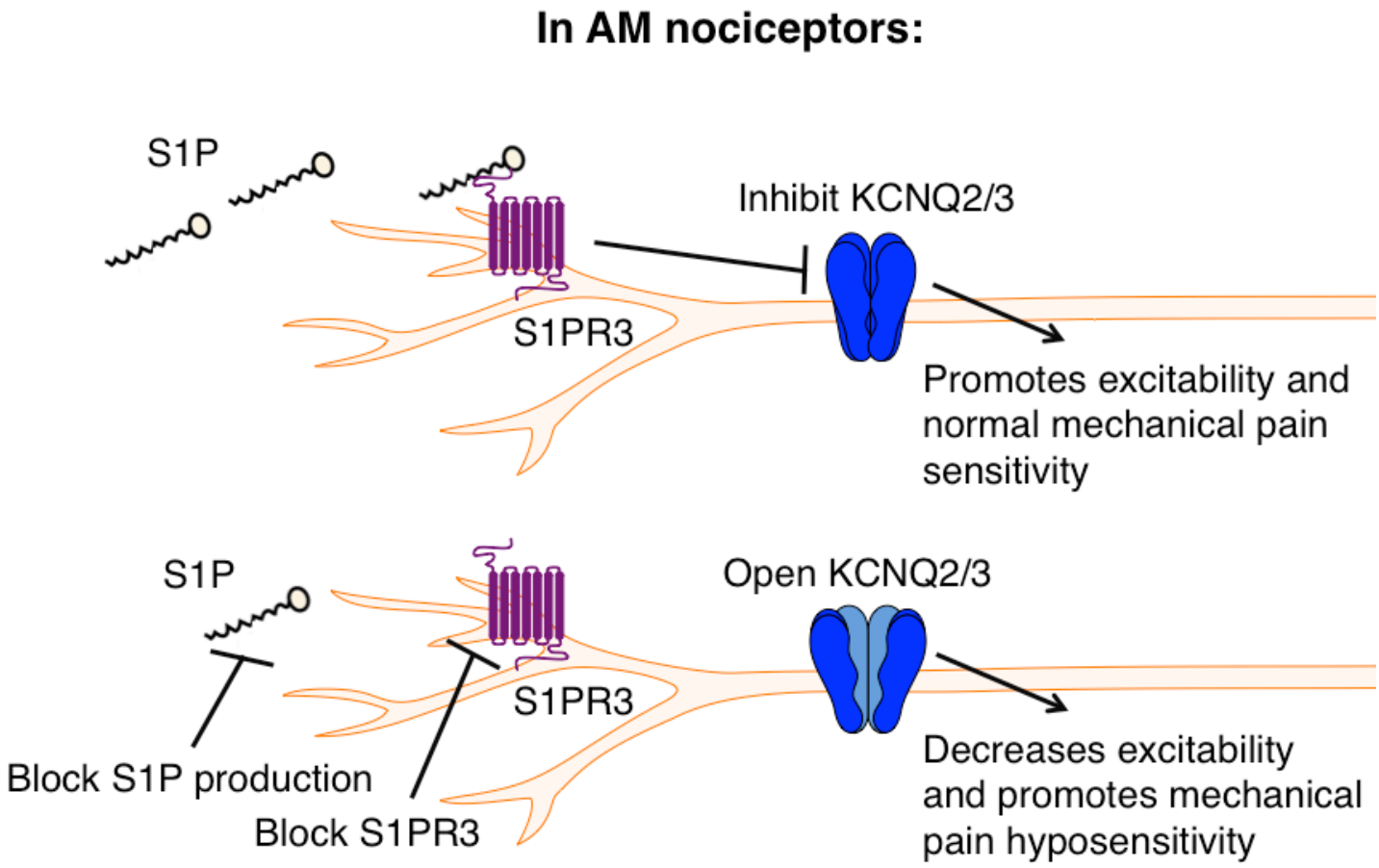

Figure 6. Proposed model illustrating a key role for S1PR3 in regulating mechanical pain in AM nociceptors. S1P promotes activation of S1PR3, which leads to inhibition of KCNQ2/3 currents and promotes normal mechanical pain sensitivity. Diminished S1P or S1PR3 antagonism alleviates inhibition of KCNQ2/3, leading to mechanical pain hyposensitivity.

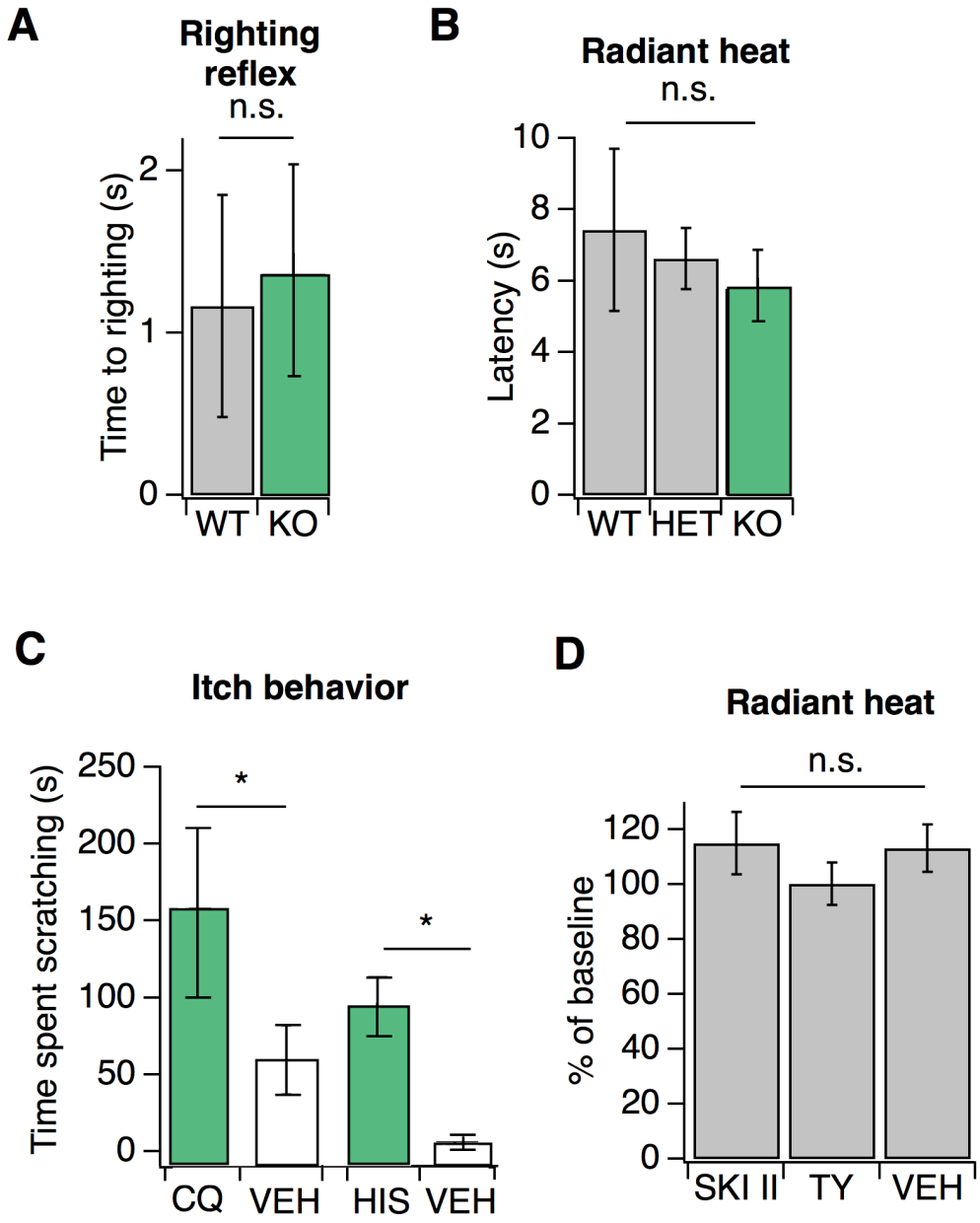

Figure S1. Loss of S1PR3 or S1P selectively impairs mechanonociception. *Related to Figure 2*. A. Time to righting in seconds for N = 6 P7 pups per genotype for WT and KO mice; $p = 0.575$ (two-tailed unpaired t-test). B. Baseline radiant heat measurements for WT, HET, and KO mice. N = 8 WT, 3 HET, and 5 KO mice. 3 measurements from both paws were averaged for each mouse. $p = 0.444$ (one-way ANOVA). C. (Left) Time spent scratching in response to injection of 50 mM chloroquine or PBS vehicle (VEH) in KO mice; $p = 0.042$ (unpaired t-test; N = 3,4 mice). (Right) Time spent scratching in response to injection of 27 mM Histamine or 0.1% DMSO-PBS in KO mice; $p = 0.019$ (unpaired t-test; N = 3,4 mice). D. Normalized paw withdrawal latencies post-injection of SKI II, TY 52156, or 0.1% DMSO-PBS vehicle into the hind paw of wild-type animals; $p = 0.65$ (one-way ANOVA); N = 5 mice per group. Unless otherwise indicated, error bars represent mean ± SD.

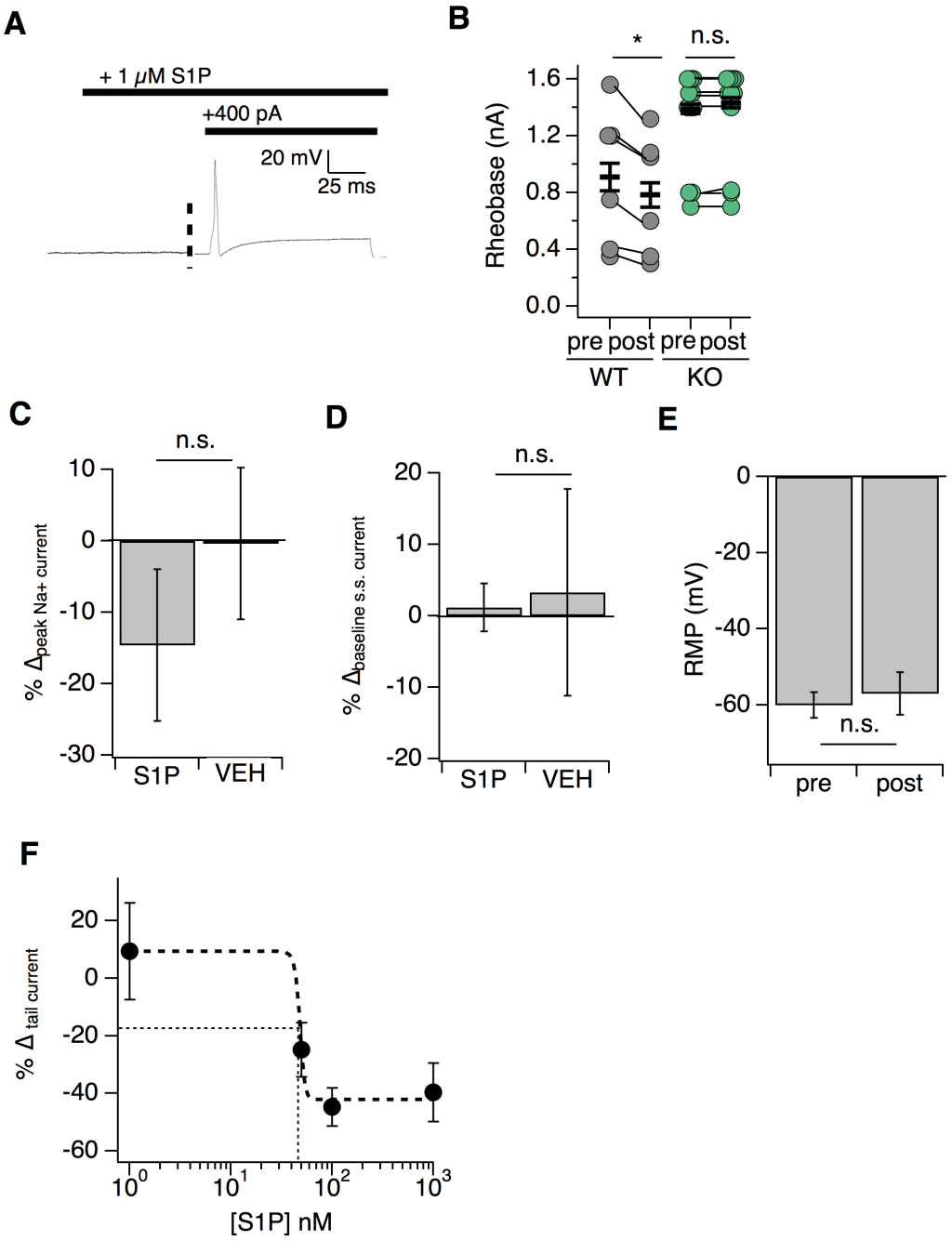

Figure S2. S1P selectively modulates potassium tail currents to increase DRG neuron excitability. *Related to Figure 5.* A. Example trace of a single mCherry+ neuron in S1P before and after current injection. B. Rheobase pre- and post-S1P application in DRG neurons; p_{WT} = 0.011; p_{KO} = 0.28 (two-tailed paired t-test). Same data are represented in Figure 5A. C. % Δ in instantaneous sodium current after S1P or 1% DMSO vehicle application for medium-diameter mCherry+ neurons; p = 0.39 (two-tailed paired t-test; N = 7 cells per group). D. % Δ in steady-state current after S1P or 1% DMSO vehicle application for medium-diameter mCherry+ neurons; p = 0.948 (two-tailed paired t-test; N = 7 cells per group). E. Resting membrane potential (RMP) in millivolts before and after addition of S1P (p = 0.23; two-tailed paired t-test; N = 6 cells). F. Dose-response relationship between % Δ in tail current and S1P concentration for 1 nM, 50 nM, 100 nM, and 1 μM S1P (N = 7 cells). EC_{50} (48.8 nM), marked by thin dotted lines, was estimated from sigmoidal fit (thick dotted line).